

Experimental and numerical modeling of liposome congregation in meteorite craters of Early Earth

Vladimir M. Subbotin,^{1,2,*} Benjamin A. Turner,¹ Brian A. Davies,¹ Alric G. Lopez,¹ and Gennady Fiksel²

¹*Arrowhead Pharmaceuticals Inc., Madison, WI, USA*

²*University of Wisconsin, Madison, WI, USA*

This paper provides experimental and numerical evidence supporting the occurrence of liposome congregation at the floors of meteor craters on Early Earth. This work builds on our earlier research, which demonstrated that liposomes submerged in a shallow Archean pond are protected from harmful UV radiation. This protection allows them to survive long enough for autocatalytic replication of amphiphiles and for mutation and selection of assemblies that maximize membrane stability. For liposomes to fuse, grow, exchange contents and membranes, and divide, they need to establish a population, which means forming a dense conglomerate that enables close physical contact. The study demonstrates that such a congregation is feasible in bowl-shaped meteor craters on Early Earth, especially under periodic seismic disturbances.

Keywords: Origin of life, liposomes, Darwinian evolution, meteor craters, earthquakes

I. INTRODUCTION

In our earlier publication [1] we proposed a hypothesis on the Darwinian evolution of liposomes based solely on natural and ever-present phenomena: solar UV radiation, the day/night cycle, gravity, and the formation and release of amphiphiles in aqueous media. The hypothesis is based on the premise that amphiphilic molecules introduced into Archean water inevitably accumulate at the water-air interface and form Langmuir layers, bilayers, and liposomes.

In our scenario, the newly formed liposomes would inevitably be destroyed by solar UV unless they acquire negative buoyancy by capturing heavy solutes, such as ribose, and descend from the water-air boundary. We have also shown that some primordial water constituents, such as ferric salts, can provide UV attenuation sufficient to shield liposomes at depths of only a few millimeters [2, 3]. The submerged liposomes, shielded from damaging UV radiation, acquire the longevity necessary to enhance autocatalytic replication of amphiphiles, their mutation, and the selection of those amphiphilic assemblies that provide the greatest membrane stability. These two sets of adaptive compositional information - heavy content and amphiphilic assemblies design induce selective pressures and promote variation in inherited adaptive traits. They also ensure liposomal survival and create an opportunity for Darwinian evolution.

However, liposome survival alone, while necessary, is not sufficient to be a subject of Darwinian evolution. For that, the surviving liposomes must form a population [4–7]. It is worth noting that although Charles Darwin did not use the term “population”, his book “The Origin of Species ...” [8] undoubtedly contains the concept of a population. For example, in Chapter II, p.45 and Chapter IV, p.84, Darwin writes: “These individual differences

are highly important for us, as they afford materials for natural selection to accumulate, it may be said that natural selection is daily and hourly scrutinizing, throughout the world, every variation, even the slightest; rejecting that which is bad, preserving and adding up all that is good.” The wordings “adding up” and “individual differences” make sense only at the population level, not at the level of single individuals. Contemporary analyses also emphasized that a population, or the formation of groups of similar entities, such as protocells, arising through temporal and spatial congregation, is fundamental for the Origin of Life [9]. Therefore, for the liposomes to be subject to Darwinian evolution, they must congregate and form a population.

Multiple in-vitro studies showed that liposomes, when subjected to physical contact with each other, undergo fusion and growth [10–13], exchange of liposomal content and membranes molecules [14–17], and fusion and division [18–20]. The issue we are trying to address in this study is: how might such a liposomal population be formed if liposomes are just scattered on the floor of primordial ponds?

Various studies [21–24] demonstrated that sites of meteorite impacts could be seeded with amphiphiles, phospholipid precursors, and ribose [25–28], the molecules that are essential for our hypothesized origin of life [1]. More so, a recent experimental study demonstrated that the meteorite impacts themselves produce phospholipid precursors directly from Earth’s soil, in both wet and dry conditions [24]. Therefore, it is plausible to consider that meteorite craters on Hadean Earth could have been potential sites for the self-sustained Darwinian evolution of liposomes [29, 30].

But what about forming a population? Meteorite craters, as shown by surface images of the Moon and Mars, exhibit a wide range of shapes and sizes [30]. Generally, their topography consists of concave, bowl-shaped depressions, dips, and crevices at scales ranging from tens of kilometers to meters and less. Each of these features, filled with water enriched with various minerals, partic-

* Email: vsubbotin@arrowheadpharma.com

ularly ferric salts, can serve as a site for liposome formation, survival, and growth. Although the concave shape of the sites theoretically encourages heavy liposomes to settle at the bottom by minimizing gravitational potential energy, this process is often impeded by friction and physical obstacles. However, external disturbances, such as local earthquakes and shock waves produced by meteorite bombardment, may shift the soil, thereby releasing liposomes and facilitating their downward migration. To explore this problem, we developed experimental and numerical models of liposomal dynamics within meteorite craters subjected to sudden, repetitive displacements.

The paper is organized as follows. Section II describes the experimental setup and results. Section III describes numerical simulations of the experiments. Section IV illustrates how liposomes are protected against UV damage in the crater environment. Section V summarizes the results.

II. EXPERIMENT

A. Earthquake literature data

The experiment described in this section is designed and built to closely simulate the ground motion characteristics observed during earthquakes, such as the soil displacement magnitude and velocity. Detailed earthquake data, including amplitude and frequency spectra of various tremor types, can be found in [31]. Displacement measurements, assembled from data across multiple earthquake sites, vary from centimeters to tens of centimeters, while velocity values vary from a fraction of 1 m/s to several m/s. The experiment and numerical simulations are designed to match these characteristics.

B. Experimental setup

A “crater” model drawing is shown in Fig. 1. The crater has a spherical cap shape with a sphere radius of 200 mm, a cap radius of 80 mm, and a height of 35 mm. It is produced using water-tight 3D printing technology. The base of the crater features ridges spaced every 5 mm, each measuring 1 mm in height. The crater is filled with water into which polyethylene red liposomes-mimicking microspheres, with a diameter of $d = 350 \mu\text{m}$ and density of $\rho = 1.2 \text{ g/cm}^3$ are submerged. The purpose of the ridges is to provide physical obstacles preventing the microspheres from rolling down the hill under gravity. Clearly, neither the size and shape of the “crater” nor the size, material, and mass of the “liposomes” approach their real-life counterparts. Rather, the purpose of this experiment is a demonstration of a general principle of liquid-submerged micro-particulate dynamics, driven by gravitation and assisted by periodic disturbances. In addition, comparing the experimental and numerical results

will validate the numerical model and provide a basis for further development and improvement.

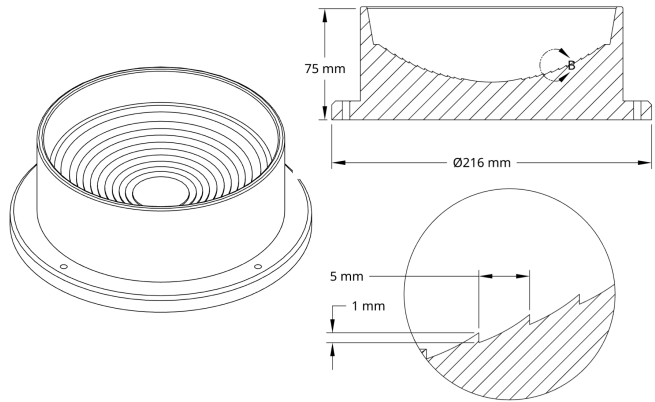


FIG. 1. A drawing of a crater model showing an overview and detail views.

An experimental setup for investigating liposome behavior is shown in Fig. 2 and consists of a stainless steel tray connected to a stand with four springs. The crater model is mounted on a 2 cm-thick wooden plate, which is positioned on top of a 3 cm-thick polyurethane foam layer that rests within the vibration stand tray. Two weights are dropped from $h = 25 \text{ cm}$, thereby generating the crater’s displacement through momentum transfer, thus emulating an initial quake jolt.

Since the foam offers minimal resistance at the initial moment, the crater velocity at impact can be estimated using momentum conservation

$$V_c = V_w \frac{M_w}{M_w + M_c + M_b}, \quad (1)$$

where M_w , M_c , and M_b are the masses of the drop weights, the crater, and the board, respectively, and V_w is the drop weight velocity at the impact.

As measured, $M_c + M_b = 1.9 \text{ kg}$ and a calculated value of $V_w = \sqrt{2gh} = 2.2 \text{ m/s}$. Two kinds of drop weights were used - steel bars with a total mass of $M_w = 2.4 \text{ kg}$, and aluminum bars with a total mass of $M_w = 0.83 \text{ kg}$. Applying Eq. 1 results in the velocity of the crater at the impact being $V_c = 1.2 \text{ m/s}$ and $V_c = 0.67 \text{ m/s}$, respectively. The impact velocity figures align well with the earthquake data presented in Section II A.

C. Experimental results

Before each test, the red microspheres were spread approximately evenly across the entire crater area. Afterwards, a series of repeated weight drops was performed, and the movement of the particles was recorded on video. The results are summarized in Fig. 3. The top and bottom rows compare results for steel and aluminum rods,

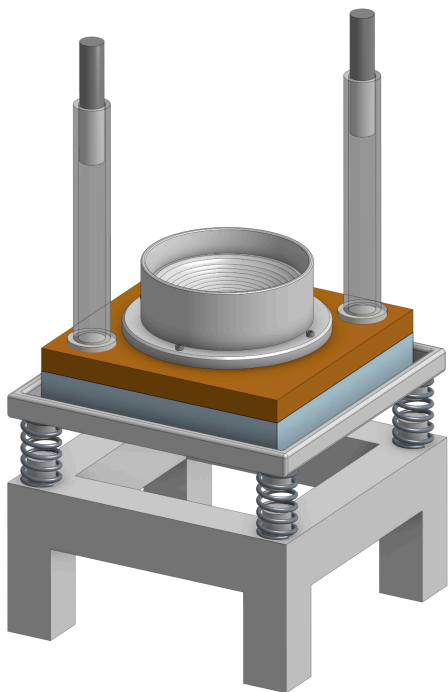


FIG. 2. Experimental setup. A stainless steel tray is connected to a stand with four springs. The crater model is mounted on a 2 cm-thick wooden plate, which is positioned on top of a 3 cm-thick soft foam layer that rests within the vibration stand tray. Two weights are dropped from $h = 25$ cm.

respectively, while the left and right columns show the initial and final stages. Dropping steel rods leads to nearly complete particle collection at the center after $N = 40$ drops. Dropping aluminum rods results in a profile that, although somewhat peaked, remains noticeably wide even after 80 drops.

III. NUMERICAL SIMULATIONS

The behavior of the microspheres (called particles in the code) in the experiment is modeled using COMSOL[®] Multiphysics software [32]. The simulation geometry shown in Fig. ?? duplicates the experimental model exactly, except that the simulations are conducted in 2D.

A thousand "numerical" particles, each with a diameter of $d = 350 \mu\text{m}$ and density of $\rho = 1.2 \text{ g/cm}^3$ are submerged in water (cyan) and are initially uniformly distributed across the curved bottom, as shown in the red circles. It is assumed that after the weights impact the crater, the crater descends and then rebounds, striking the particles and initiating their motion. Because of the concave shape of the bottom, the momentum transmitted to the particles will have both vertical and horizontal components, depending on their initial positions, as indicated by the arrows. Specifically, the horizontal velocity component of each particle is $V_0 \sin(2\alpha)$ and the

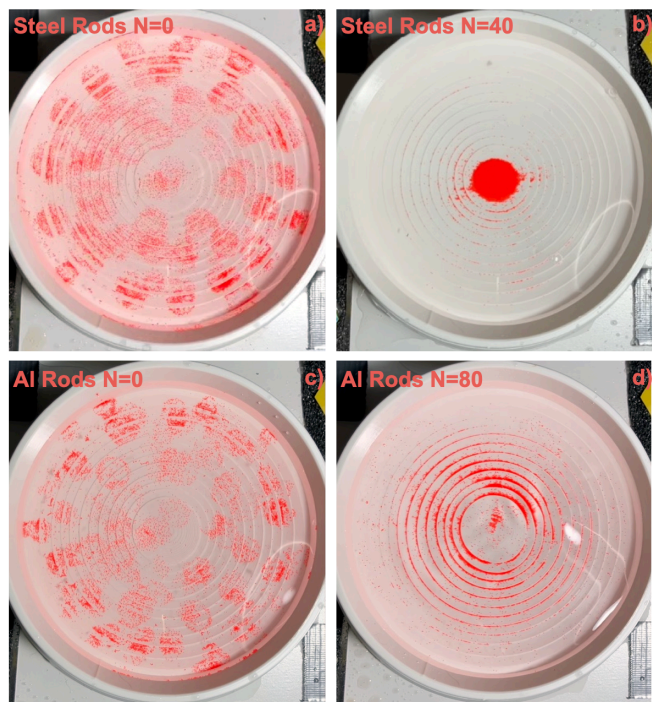


FIG. 3. Summary of particle dynamics. The top and bottom rows compare results for steel and aluminum rods, respectively, while the left and right columns show the initial and final stages. (b) Dropping steel rods leads to nearly complete particle collection at the center after $N = 40$ drops. (d) Dropping aluminum rods results in a profile that, although somewhat peaked, remains noticeably wide even after 80 drops.

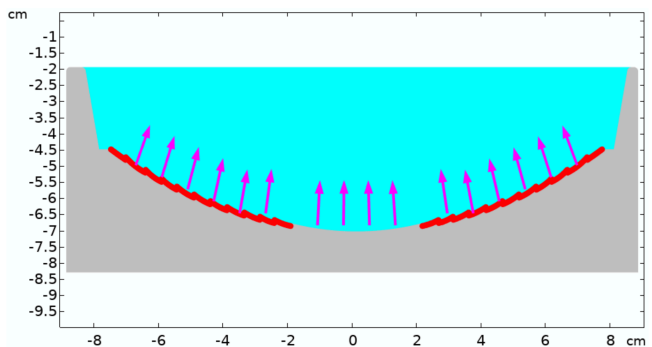


FIG. 4. A thousand particles, each with a diameter of $d = 350 \mu\text{m}$ and density of $\rho = 1.2 \text{ g/cm}^3$ are submerged in water (cyan) and are initially uniformly distributed across the curved bottom, as shown in the red circles. It is assumed that after the weights impact the crater, the crater descends and then rebounds, striking the particles and initiating their motion. Because of the concave shape of the bottom, the momentum transferred to the particles has both vertical and horizontal components, depending on their initial positions, as indicated by the arrows.

vertical component is $V_0(1 + \cos(2\alpha))$, where V_0 is the crater rebound velocity and $\sin \alpha = x/R$, where x is the particle horizontal position at the impact and R is the radius of the concave cavity. The exact value of the rebound velocity V_0 is not known, but is likely a fraction of the crater impact velocity V_c due to some energy dissipation during compression and rebound. To investigate the effect of the rebound velocity, it was varied from 0.1 m/s to 1.0 m/s.

The motion of each particle is governed by gravity, buoyancy, and viscous friction

$$m \frac{d\vec{v}}{dt} = m\vec{g} \frac{\rho - \rho_w}{\rho_w} - m \frac{\vec{v}}{\tau_\mu}, \quad (2)$$

where m , \vec{v} , and ρ are the particle mass, velocity and density, and τ_μ is the characteristic viscous time

$$\tau_\mu = \frac{\rho d^2}{18\mu}, \quad (3)$$

where d is the particle's diameter and μ is the water viscosity. For $\rho = 1.2 \text{ g/cm}^3$, $d = 350 \text{ }\mu\text{m}$, and $\mu = 10^{-3} \text{ Pa}\cdot\text{s}$, $\tau_\mu = 8.2 \text{ ms}$. The short viscous time means that, after an initial impulse, a particle comes to a standstill in just a few milliseconds. An approximate calculation of the distance traveled by a particle with an initial velocity of 0.5 m/s is $l = 4 \text{ mm}$, suggesting that traveling from the cavity edge at $r = 8 \text{ cm}$ to the center requires at least 20 jolts or even more if only a fraction of the velocity is directed horizontally and gravity-induced deviations from horizontal motion are considered.

Figure 5 shows the particle distribution over the bottom of the cavity after consecutive 60 impacts at a rebound velocity of 0.5 m/s. A clear concentration enhancement is visible in the central area of the cavity. To explore the effect of the rebound velocity, it was varied from $V_0 = 0.1 \text{ m/s}$ to 1.0 m/s. The result shown in Fig. 6 confirms the quantitative estimates for the number of impacts needed. Indeed, according to the simulations, collecting 70% of all particles at a rebound velocity of $V_0 = 0.5 \text{ m/s}$ takes about 20 impacts, while reaching 90% of all the particles requires approximately 30 impacts, which aligns well with the estimates. Overall, the numerical results are in good agreement with the experimental data.

IV. LIPOSOME PROTECTION AGAINST UV DESTRUCTION IN CRATER GEOMETRY

While the mechanism by which ferric salts protect liposomes from UV damage has been explained and quantified in our earlier publications [1–3], this section focuses on visually demonstrating this effect within the crater geometry.

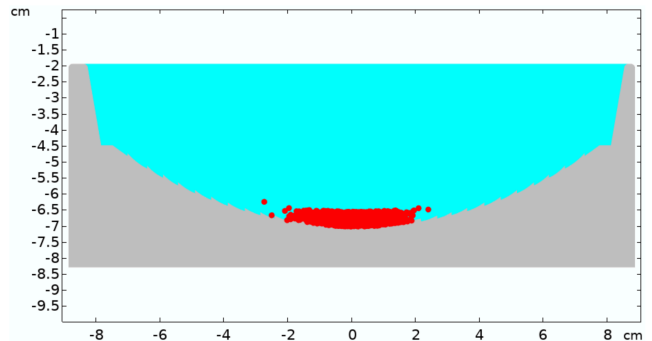


FIG. 5. Particle distribution over the bottom of the cavity after 60 impacts at a rebound velocity of 0.5 m/s.

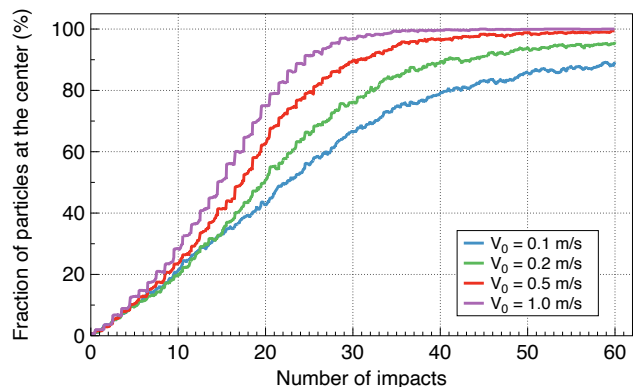


FIG. 6. Evolution of particle concentration at the center at various rebound velocities V_0 . Shown is the time dependence of the fraction of the particle at the central area of the cavity $r < 2 \text{ cm}$. The small wiggles correspond to brief movements toward the center following each impact.

We used large polymerizable UV-sensitive multilamellar liposomes with an average diameter of $1.64 \text{ }\mu\text{m}$ composed of Dibehenoyl-sn-glycero-3-phosphocholine (DBPC) and a 10,12-Pentacosadiynoic acid (PCDA) with a DBPC: PCDA molar ratio of 80:20, at a total lipid concentration of 7 mM (Encapsula NanoSciences, Brentwood, TN, USA). Liposomes were assembled in a sucrose solution, allowing them to achieve a specific density of 1.014 g/cm^3 .

The crater has a geometry very similar to that used in Section II B, except being fabricated in a planar geometry and with a transparent front wall. The steps on the crater's floor are 2.5 mm high and spaced 5 mm apart. The crater was slowly filled to a depth of 30 mm with a solution of iron trichloride at a concentration of 0.2 g/L and a specific density of 1.001 g/cm^3 via a stainless steel tubing inserted in the lowest point. The infusion speed was 1 mL/min, and the total volume of solution was 94 mL. The outermost steps were intentionally left uncovered. The solution's yellowish tint, as shown in the photo, re-

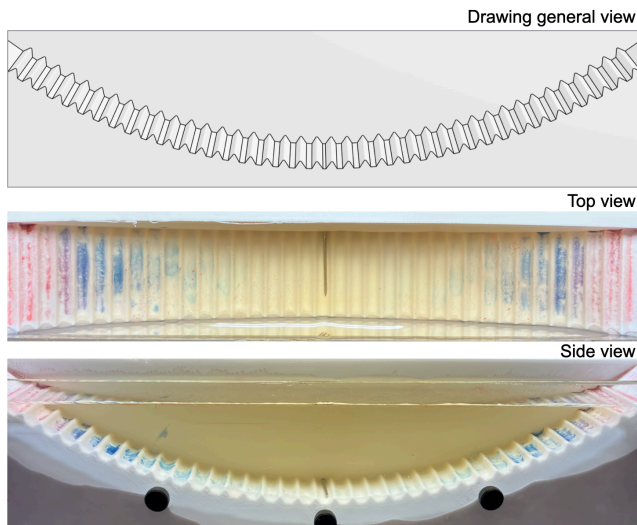


FIG. 7. Illustration of liposome protection from UV. The top panel shows a drawing of the crater. The top- and side-view photographs show the intensity distribution of the blue color after UV exposure. When subjected to UV radiation, the liposomes go through a color change from the original white to blue, with the color intensity correlated with the level of physical destruction of the liposomes. Furthermore, the liposomes change to red when exposed to high heat. The experiment shows that liposomes located at the edges and not covered by the solution turn to blue and then to red within the first few seconds of UV exposure, likely due to the combined effects of UV and heat emitted from the lamp. Liposomes covered by the solution demonstrate a gradual change of the blue color from deep-blue for those at the edge to less intense and almost transparent, deeper toward the center. Even after more than two hours of UV exposure, the liposomes in the crater’s center stayed intact.

sults from the oxidation of iron.

A low-pressure UV bulb (Spectrolite, 15 W, arc length 35 cm) was positioned 30 mm above the crater. When subjected to UV radiation, the liposomes go through a color change from the original white to blue [33] with the color intensity correlated with the level of physical destruction of liposomes, as was tested and confirmed by the liposome manufacturer. Furthermore, the liposomes change to red when exposed to high heat. The experiment shows that liposomes located at the edges and not covered by the solution turn to blue and then to red

within the first few seconds of UV exposure, likely due to the combined effects of UV and heat emitted from the lamp. Liposomes covered by the solution demonstrate a gradual change of the blue color from deep-blue for those at the edge to less intense and almost transparent, deeper toward the center. Even after more than two hours of UV exposure, the liposomes in the crater’s center stayed intact.

V. SUMMARY AND CONCLUSIONS

Various in-vitro studies have demonstrated that when liposomes come into physical contact, they tend to fuse, grow, exchange contents, and divide. We hypothesize that gravity-driven and earthquake-assisted movement of liposomes within meteoric craters on Early Earth could lead to their accumulation at the crater floor. The paper presents both experimental and numerical investigations that demonstrate this phenomenon.

The “crater” for this experiment is modeled as a spherical cap shape with a sphere radius of 200 mm and a cap radius and height of 80 mm and 35 mm, respectively, and printed using water-tight 3D printing technology. The base of the crater features ridges spaced every 5 mm, each measuring 2.5 mm in height. The crater is filled with water into which fluorescent red plastic “liposomes”, with a diameter of $d = 350 \mu\text{m}$ and density of $\rho = 1.2 \text{ g/cm}^3$ are submerged. The purpose of the ridges is to provide physical obstacles preventing the microspheres from rolling down the hill under gravity.

Clearly, neither the size and shape of the “crater” nor the size, material, and mass of the “liposomes” correspond to their real-life counterparts. Rather, the purpose of this experiment is a demonstration of a general principle of liquid-submerged micro-particulate dynamics, driven by gravitation and assisted by periodic disturbances. Both experimental and numerical results show that applying a series of jolts with a magnitude similar to actual earthquakes causes the particle profile to gradually redistribute, eventually forming a density profile that peaks at the center.

ACKNOWLEDGMENTS

The authors thank Dr. Zahra Mirafzali (Encapsula NanoSciences, Brentwood, TN, USA) for fulfilling our request to produce heavy UV-sensitive liposomes and for generously providing additional liposomes.

-
- [1] V. Subbotin and G. Fiksel, Exploring the lipid world hypothesis: a novel scenario of self-sustained darwinian evolution of the liposomes, *Astrobiology* **23**, 344 (2023).
 [2] V. Subbotin and G. Fiksel, Aquatic ferrous solutions of prebiotic mineral salts as strong uv protectants and possible loci of life origin, *Astrobiology* **23**, 741 (2023).

- [3] B. Turner *et al.*, Protection of liposomes by ferric salts against the uv damage and its implications for the origin of life, *Frontiers in Astronomy and Space Sciences* **12**, 1566396 (2025).
 [4] P. Adamski *et al.*, From self-replication to replicator systems en route to de novo life, *Nature Reviews Chemistry* **4**, 386 (2020).

- [5] M. S. Mariano and J. F. Fontanari, Evolutionary game-theoretic approach to the population dynamics of early replicators, *Life* **14**, 1064 (2024).
- [6] S. Okasha, The major transitions in evolution—a philosophy-of-science perspective, *Frontiers in Ecology and Evolution* **10**, 793824 (2022).
- [7] N. Takeuchi and P. Hogeweg, Multilevel selection in models of prebiotic evolution ii: a direct comparison of compartmentalization and spatial self-organization, *PLOS Computational Biology* **5**, e1000542 (2009).
- [8] C. Darwin, *On the Origin of Species by Means of Natural Selection, or the Preservation of Favoured Races in the Struggle for Life*, 1st ed. (John Murray, London, 1859).
- [9] E. Szathmáry and L. Demeter, Group selection of early replicators and the origin of life, *Journal of Theoretical Biology* **128**, 463 (1987).
- [10] J. Connor, M. B. Yatvin, and L. Huang, pH-sensitive liposomes: acid-induced liposome fusion, *Proceedings of the National Academy of Sciences* **81**, 1715 (1984).
- [11] S. Deshpande *et al.*, Membrane tension-mediated growth of liposomes, *Small* **15**, 1902898 (2019).
- [12] S. Nir *et al.*, Aggregation and fusion of phospholipid vesicles, *Progress in Surface Science* **13**, 1 (1983).
- [13] H. Noguchi and M. Takasu, Fusion pathways of vesicles: a brownian dynamics simulation, *The Journal of Chemical Physics* **115**, 9547 (2001).
- [14] Y.-H. M. Chan, B. van Lengerich, and S. G. Boxer, Lipid-anchored dna mediates vesicle fusion as observed by lipid and content mixing, *Biointerphases* **3**, FA17 (2008).
- [15] M. M. Hanczyc, S. M. Fujikawa, and J. W. Szostak, Experimental models of primitive cellular compartments: encapsulation, growth, and division, *Science* **302**, 618 (2003).
- [16] M. D. Hardy *et al.*, Self-reproducing catalyst drives repeated phospholipid synthesis and membrane growth, *Proceedings of the National Academy of Sciences* **112**, 8187 (2015).
- [17] P. Yang, R. Lipowsky, and R. Dimova, Nanoparticle formation in giant vesicles: synthesis in biomimetic compartments, *Small* **5**, 2033 (2009).
- [18] S. Deshpande *et al.*, Mechanical division of cell-sized liposomes, *ACS Nano* **12**, 2560 (2018).
- [19] H.-G. Döbereiner *et al.*, Budding and fission of vesicles, *Biophysical Journal* **65**, 1396 (1993).
- [20] S. Penič *et al.*, Budding and fission of membrane vesicles: A mini review, *Frontiers in Physics* **8**, 342 (2020).
- [21] D. W. Deamer and R. Pashley, Amphiphilic components of the murchison carbonaceous chondrite: surface properties and membrane formation, *Origins of Life and Evolution of the Biosphere* **19**, 21 (1989).
- [22] J. P. Dworkin *et al.*, Self-assembling amphiphilic molecules: Synthesis in simulated interstellar/precometary ices, *Proceedings of the National Academy of Sciences* **98**, 815 (2001).
- [23] Z. Martins and M. A. Pasek, Delivery of organic matter to the early earth, *Elements* **20**, 19 (2024).
- [24] J. Zhao and K. Mimura, Supply of phospholipid precursors and evolution sites on the early earth by impact, *Geochimica et Cosmochimica Acta* (2025).
- [25] S. Abe *et al.*, Gamma-ray-induced synthesis of sugars in meteorite parent bodies, *ACS Earth and Space Chemistry* **8**, 1737 (2024).
- [26] Y. Furukawa *et al.*, Extraterrestrial ribose and other sugars in primitive meteorites, *Proceedings of the National Academy of Sciences* **116**, 24440 (2019).
- [27] C. Ono *et al.*, Abiotic ribose synthesis under aqueous environments with various chemical conditions, *Astrobiology* **24**, 489 (2024).
- [28] K. Paschek *et al.*, Possible ribose synthesis in carbonaceous planetesimals, *Life* **12**, 404 (2022).
- [29] C. S. Cockell, The origin and emergence of life under impact bombardment, *Philosophical Transactions of the Royal Society B* **361**, 1845 (2006).
- [30] G. Osinski *et al.*, The role of meteorite impacts in the origin of life, *Astrobiology* **20**, 1121 (2020).
- [31] B. Mohraz and F. Sadek, Earthquake ground motion and response spectra, in *The Seismic Design Handbook*, edited by F. Naeim (Springer US, Boston, MA, 2001) pp. 47–124.
- [32] *COMSOL 5.5, COMSOL AB, Stockholm, Sweden* (2019).
- [33] D. Ahn, S. Lee, and J.-M. Kim, Rational design of conjugated polymer supramolecules with tunable colorimetric responses, *Advanced Functional Materials* **19**, 1483 (2009).